minerals

MDPI

Article

Ion-Specific Effects on Bubble Coalescence: A Cohesive Pressure Approach to SDS Foam Stability

Stoyan I. Karakashev [1,*], Yunus Emre Çavdar [2], Orhan Ozdemir [2,*], Nikolay A. Grozev [3], Kristina Mircheva [3], Stanislav Donchev [2], Christomir Christov [4], Tsvetan Tsenov [5], Dilyana Ivanova-Stancheva [2] and Irina Yotova [2]

1 Faculty of Natural Sciences, University of Shumen, 9700 Shumen, Bulgaria
2 Department of Mineral Processing Engineering, Faculty of Mines, Istanbul Technical University, 34469 Istanbul, Türkiye; cavdar@itu.edu.tr (Y.E.Ç.); st.donchev@shu.bg (S.D.); d.ivanova@shu.bg (D.I.-S.); i.yotova@shu.bg (I.Y.)
3 Department of Physical Chemistry, Sofia University, 1 James Bourchier Avenue, 1164 Sofia, Bulgaria; fhng@chem.uni-sofia.bg (N.A.G.); fhkm@chem.uni-sofia.bg (K.M.)
4 University of Ruse, 8 Studentska Street, 7017 Ruse, Bulgaria; christovshumen@gmail.com
5 Department of Ecology and Environmental Protection, Faculty of Shipbuilding, Technical University of Varna, 1 "Studentska" Str., 9010 Varna, Bulgaria; tzvetan.tsenov@tu-varna.bg
* Correspondence: s.karakashev@shu.bg (S.I.K.); orhanozdemir@itu.edu.tr (O.O.)

Abstract

This work investigates the effect of specific electrolytes (NaCl, KCl, $MgCl_2$, and $CaCl_2$) on bubble coalescence and the stability of the resulting foam caps in aqueous sodium dodecyl sulfate (SDS) solutions. At low concentrations, we observe that all electrolytes studied exhibited a similar effect on bubble coalescence, driven primarily by the electrostatic screening of the repulsion between bubbles. However, a distinct divergence in behavior emerges at higher concentrations: KCl and $CaCl_2$ destabilize the foam, while NaCl and $MgCl_2$ act as foam boosters. By applying Pitzer's theory and the concept of cohesive pressure, we propose that foam stability is governed by the hydration compatibility between the surfactant head groups and the salt ions. We describe a mechanism in which the "cohesive pressure" of the water matrix determines the efficiency of the SDS adsorption layer. Specifically, strong kosmotropic ions (e.g., Mg^{2+}) preserve the hydration shell of the sulfate head groups, thereby preventing film collapse, whereas ions with lower dehydration energy (e.g., Ca^{2+}) are proposed to facilitate the formation of contact ion pairs, thereby promoting rapid coalescence.

Keywords: SDS foam stability; cohesive pressure; Pitzer's theory; bubble coalescence; ion-specific effects; Collins' rule

Academic Editor: Hyunjung Kim

Received: 15 June 2026
Revised: 29 June 2026
Accepted: 6 July 2026
Published: 10 July 2026

1. Introduction

The stability of aqueous foams is of paramount importance in numerous industrial sectors, particularly in mineral flotation, where the recovery of valuable minerals depends on the efficient formation and stability of bubble aggregates [1]. Sodium dodecyl sulfate (SDS), an anionic surfactant, has long been used as a canonical model system for exploring surface phenomena [2–13]. Despite extensive research, the mechanism by which electrolytes affect the stability of SDS foam remains a subject of intense academic debate. Historically, the stability of surfactant films has primarily been interpreted through the prism of DLVO theory, focusing on the electrostatic screening of the electric double layer [14–16]. While this model provides an adequate description at low electrolyte concentrations, it often fails to account

for the complex, ion-specific behaviors observed at higher ionic strengths; these phenomena are typically associated with the Hofmeister series [17–20]. These deviations indicate that the background electrolyte does not act solely as a screening agent; rather, it fundamentally alters the thermodynamic properties of the bulk aqueous phase, affecting the efficiency of the adsorption layer. A critical element in these interactions is the hydration shell of the ions and their compatibility with the surfactant head groups. As Collins proposed in his "Law of Matching Water Affinities," the strength of the interaction between oppositely charged ions is intrinsically linked to their relative hydration energies, which determine whether an ion-pair forms [21–23]. Furthermore, Pitzer's theory provides a robust mathematical framework for calculating the activity coefficients of electrolyte solutions by accounting for both electrostatic and non-electrostatic short-range interactions [24–27].

This work aims to provide a unified explanation for the divergent behavior of different electrolytes that function as foam stabilizers or destabilizers by integrating these theoretical concepts with the notion of "cohesive pressure". Specifically, we investigate how the cohesive pressure of the water matrix modulates the energy required to create a cavity for the surfactant molecule, thereby advancing the understanding of bubble coalescence in complex saline environments.

A mechanistically important, but often neglected, aspect of these systems is the molecular-scale structure of the aqueous phase. In concentrated electrolyte solutions, the average interionic distance decreases to the point where no "bulk water" remains in the classical sense. Marcus [28] demonstrated that at concentrations of 3–6 mol/dm^3, the gap between adjacent ions is smaller than the diameter of a water molecule (0.276 nm), rendering the standard concept of independent ion hydration shells physically meaningless. Under such conditions, water molecules are simultaneously polarized by both cations and anions, and their hydrogen-bonding dynamics are profoundly disrupted. This structural transformation of the aqueous phase has direct consequences for the thermodynamic properties governing surfactant adsorption and foam stability.

The ion-specific nature of these effects is encoded in quantifiable physical properties of the ions. Marcus [29] established that the increase in molar ionic surface tension k_i (the degree to which an individual ion depletes or enriches the air/water interface) correlates with the ion's size, polarizability, softness, and water-structuring capacity. Kosmotropic ions (high k_i, e.g., Mg^{2+}, SO_4^{2-}) are depleted from the surface and strengthen the bulk water network, while chaotropic ions (low or negative k_i, e.g., I^-, Cs^+) accumulate at the interface and weaken it., The relevant k_i values for the salts studied here are: Na^+ = 1.20, K^+ = 1.10, Mg^{2+} = 2.25, Ca^{2+} = 2.10, Cl^- = 0.90 mN m^{-1} M^{-1} [29]. These increments directly determine how each electrolyte modifies the energetics of the air/water interface in the presence of SDS.

The macroscopic manifestation of ion-specific hydration in bulk solution is captured by the Setchenow (salting-out) constant K_s, which quantifies the reduction in solubility of a nonpolar solute per unit increase in electrolyte concentration. Marcus [30] showed that K_s values are additive with respect to ionic contributions and scale with the difference between the conventional standard partial molar volume of an ion and its intrinsic volume; this quantity is directly related to the electrostriction the ion exerts on surrounding water. The values used in the present work (NaCl: 0.20, KCl: 0.15, $MgCl_2$: 0.40, $CaCl_2$: 0.33 M^{-1}) reflect this ionic electrostriction hierarchy and are consistent with the independent analysis of Ni and Yalkowsky [31], which showed that K_s correlates with the octanol–water partition coefficient of the nonpolar solute, confirming that the salt effect operates through modulation of the aqueous phase polarity rather than direct solute–ion interaction.

The role of the hydrophobic effect, the thermodynamic penalty paid when a nonpolar moiety is inserted into the hydrogen-bonded water network, provides a molecular founda-

tion for the cavitation work concept central to this study. Hummer et al. [32] developed an information-theory framework showing that the excess chemical potential of a hard-sphere solute in water is determined entirely by the probability of finding a suitably sized cavity in the solvent, which in turn depends on the density and oxygen–oxygen pair distribution function of bulk water. Their analysis demonstrated that this cavity formation free energy increases monotonically with solute size and is sensitive to changes in water density and compressibility, properties that are precisely modified by dissolved electrolytes. Adding NaCl to water increases the excess chemical potential of a methane-sized cavity by approximately 10 kJ/mol at 5 mol/dm^3 [32], providing quantitative molecular-level support for the cohesive pressure mechanism proposed in the present work.

The identity of the counter-ion of a dodecyl sulfate surfactant profoundly influences its micellar and interfacial properties. Pandey et al. [33] systematically compared LiDS, NaDS, CsDS, and $Mg(DS)_2$ and found that surface activity increased in the order $Li^+ < Na^+ < Cs^+ < Mg^{2+}$, while foamability, governed by micellar lability, followed the opposite trend. CsDS and $Mg(DS)_2$ form highly stable micelles with long relaxation times (τ_2 = 3000 ms for CsDS vs. 1 ms for NaDS at 50 mM). The surface viscosity of the adsorbed monolayer increases in the order LiDS < NaDS < CsDS < $Mg(DS)_2$ [33], demonstrating that tighter molecular packing, driven by stronger counter-ion binding, is the primary determinant of foam film mechanical strength. These findings provide a direct experimental precedent for the divergent behavior of $NaCl/MgCl_2$ and $KCl/CaCl_2$ observed in the present study.

The ionic radii of the species studied here have been determined from ion–water inter-nuclear distances by X-ray and neutron diffraction [34], and confirm that the effective size of an ion in aqueous solution closely matches its Pauling crystal ionic radius when the electrostriction of the first hydration shell is properly accounted for. For the ions of interest: Li^+ = 0.071 nm, Na^+ = 0.097 nm, K^+ = 0.141 nm, Mg^{2+} = 0.070 nm, Ca^{2+} = 0.103 nm, Cl^- = 0.180 nm [34]. The striking similarity in the bare radii of Mg^{2+} and Li^+, despite their very different charge densities, underscores that charge density, rather than bare size, is the operative parameter in ion–surfactant interactions.

Although the Hofmeister series, Collins' Law of Matching Water Affinities, and hydration-force theory each describe ion-specific effects qualitatively, they do not provide a single quantitative measure linking the structural state of bulk water to the cavity-formation work that governs surfactant adsorption and, ultimately, bubble coalescence. Classical DLVO theory, in turn, captures electrostatic screening but not these short-range, ion-specific contributions. The extended-DLVO treatments that add non-DLVO terms to the disjoining pressure of thin films have been developed to address this gap. The novelty of the present work is to translate bulk hydration stress into an interfacial cohesive pressure through the Pitzer formalism and to use it as a unifying, semi-quantitative descriptor of the divergent foam-stabilizing and foam-destabilizing behavior of electrolytes. To probe this framework, four salts were selected to span the Hofmeister series in both valence and water affinity: two monovalent cations—Na^+, a borderline kosmotrope/chaotrope, and K^+, a chaotrope—and two divalent cations—Mg^{2+}, a strong kosmotrope, and Ca^{2+}, of intermediate character—sharing the common anion Cl^-. This minimal but deliberately contrasted set is sufficient to expose the kosmotrope/chaotrope and mono-/divalent distinctions that the cohesive-pressure model is intended to explain. We note that a broader electrolyte set, including a wider range of anions, would be required to establish the full generality of the model; this is identified as a limitation of the present study.

2. Materials and Methods

2.1. Reagents and Sample Preparation

In this experimental study, sodium dodecyl sulfate (SDS) with a purity of ≥99.0% obtained from Sigma-Aldrich (Tokyio, Japan) was employed as a surfactant. Electrolyte solutions were prepared using analytical-grade salts: NaCl, KCl, $MgCl_2$, $CaCl_2$ (Sigma-Aldrich, Søborg, Denmark), and $CaCl_2$ (Sigma-Aldrich, Taufkirchen, Germany). Deionized water with a total dissolved solids (TDS) content 0–3 ppm was used in all solution preparations. To eliminate potential surface contamination, all laboratory glassware was subjected to a cleaning protocol involving rinsing with ethanol (99% purity, MERCK, Darmstadt, Germany), followed by a final wash with deionized water and thermal drying in a clean oven (Elektro–Mag, İstanbul, Türkiye). All tests were conducted under controlled laboratory conditions at a constant room temperature of 23 ± 1 °C.

2.2. Experimental Procedures

2.2.1. Bubble Coalescence Analysis

The assessment of bubble coalescence followed the methodology described in ref. [35]. The determination of Critical Coalescence Concentration (CCC) for both pure SDS and SDS-salt mixtures was carried out in a bubble column using light-adsorption principles (see Figure 1). The apparatus consisted of a 155 cm^3 micro-flotation cell (30 × 220 mm) equipped with a porous frit (10–16 µm). Nitrogen gas was fed into the system at a constant rate of 50 cm^3/min.

Figure 1. Experimental setup for bubble coalescence measurements (**a**) Photograph of the experimental setup (**b**) Schematic representation of the experimental setup [36].

Data acquisition was achieved using a cold light source (Soif Optical Instruments, Shangai, China) paired with a Thorlabs intensity detector (Thorlabs, Newton, NJ, USA), interfaced with the Optical Power Monitor (OPM) software (v. 6.1). The measurement logic involves monitoring light attenuation approximately 10 cm above the frit, where the drop in transmitted light intensity serves as a proxy for bubble coalescence frequency. Concurrent visual documentation of bubble formation was performed via high-resolution camera imaging (Bushman Equipment Inc., Menomonee Falls, WI, USA).

2.2.2. Dynamic Foam Stability Assessment

Foam evolution and decay characteristics were quantitatively determined using a DFA100 dynamic foam analyzer (KRÜSS GmbH, Hamburg, Germany). The system utilizes a tempered glass column (40 mm diameter; 250 mm height) with integrated optical sensors for real-time monitoring. Each experimental run was initiated by introducing 100 cm^3 of the sample solution into the column. Foam was generated by injecting air at a rate of 0.2 dm^3/min through a base-mounted filter plate (pore size 12–25 µm). The height of the

foam column was recorded over a 60 s generation phase. At the 60 s mark, the air supply was automatically terminated to allow for the monitoring of the foam dissipation process over a 40 s interval. The resulting dynamic foam stability factor (Σ, in min) was calculated using Equation (1):

$$\Sigma = \frac{H_{\max} A}{Q} \quad (1)$$

where $H_{\max}$ represents the maximum observed foam height (cm), A denotes the column's cross-sectional area (cm^2), and Q signifies the gas flow rate (cm^3/min).

2.3. Theory: Thermodynamic Behavior of Concentrated Salts and Surfactant Mixtures

The theoretical treatment applied in this work was described in a previous study of ours [37]. Given its importance for this study, it is presented in more detail below. The observed experimental data regarding foam stability cannot be fully elucidated by the classical DLVO theory alone since this theory primarily addresses electrostatic double-layer interactions. To explain the divergent behavior of the electrolytes (NaCl, KCl, $MgCl_2$, $CaCl_2$) studied at higher concentrations, we employ a thermodynamic framework based on the Pitzer theory, the concept of cohesive pressure, and the Law of Matching Water Affinities (Collins' Rule).

In concentrated electrolyte solutions, the bulk thermodynamic properties of the aqueous phase are governed by ion–solvent and ion–ion interactions. To quantify the resistance of the liquid matrix to cavity formation by an amphiphilic solute such as SDS, it is necessary to define the cohesive internal pressure (Π_{coh}) of the solution.

This quantity, governed by the foundational thermodynamic equation of state [38], describes how the internal energy of the solvent varies with volume at constant temperature (Equation (2)):

$$\Pi_{coh} = \left(\frac{\partial U}{\partial V}\right)_T = T\left(\frac{\partial P}{\partial T}\right)_V - P \quad (2)$$

Here, the first term on the right-hand side represents the thermal pressure of the medium, and P denotes the external ambient pressure. The cohesive pressure reflects the total intermolecular attractive forces within the solvent, arising from hydrogen bonding and dispersion interactions among water molecules.

2.3.1. Molecular Context: The State of Water in Concentrated Electrolyte Solutions

Before developing the cohesive pressure formalism, it is instructive to establish the physical state of the aqueous medium under the relevant experimental conditions. In a 1 mol/dm^3 1:1 electrolyte solution, the average cation–anion distance is d_{av} = 0.94 nm; this value decreases to 0.63 nm at 3 mol/dm^3 [39]. For the divalent salts studied here ($MgCl_2$, $CaCl_2$ at 0.1–1 mol/dm^3), the equivalent ionic strength corresponds to concentrations at which the water molecules can no longer form unperturbed hydrogen-bonded networks between the ions. Marcus [34] demonstrated that at concentrations $\geq$3 mol/dm^3, a water molecule (diameter 0.276 nm) cannot be accommodated in a linear hydrogen-bonding geometry between adjacent ions, meaning that all water present is effectively "contact water" simultaneously interacting with multiple ionic species. This physical picture directly motivates the concept of a salt-concentration-dependent cohesive pressure: as electrolyte concentration increases, the structural state of the water matrix shifts from bulk-like to ion-dominated, and the thermodynamic cost of creating a hydrophobic cavity within it changes accordingly.

The ion-specific nature of this structural transformation is encoded in the molar ionic surface tension increments k_i [40]. An increase in the surface tension of an electrolyte, $\Delta\sigma = k_E \cdot c_E$, reflects the net depletion of ions from the surface layer relative to the bulk; this

is a direct consequence of the ions' hydration energetics. Strongly hydrated kosmotropic ions (Mg^{2+}, k_i = 2.25; Na^+, k_i = 1.20 mN m^{-1} M^{-1}) are depleted from the surface because their transfer to the less structured interfacial region would disrupt their extensive hydration shells. The Pitzer virial coefficients ($\beta^{(0)}$, $\beta^{(1)}$, C^{φ}) encode the ion-specific short-range interactions that distinguish $MgCl_2$ from $CaCl_2$ despite their identical stoichiometry. The larger $\beta^{(0)}$ for $MgCl_2$ (0.3524 kg/mol) compared to $CaCl_2$ (0.3159 kg/mol) reflects the stronger electrostriction exerted by Mg^{2+} on coordinating water molecules, consistent with its smaller ionic radius (0.070 nm) and higher charge density relative to Ca^{2+} (0.103 nm) [34]. This difference in charge density is the molecular origin of the divergent foam stability observed in Regime II.

The molecular-scale foundation for the cavitation energy term is provided by the information-theory approach of Hummer et al. (1998) [32]. Within their framework, the excess chemical potential of inserting a hard-sphere solute of exclusion radius d into water is $\mu^{ex} = -k_B T \, ln \, p_0$, where p_0 is the probability of finding an empty cavity of the required size in the bulk liquid. This probability is determined by the density ρ and the oxygen–oxygen radial distribution function g(r) of the solvent; both of these properties change substantially when electrolytes are added. Hummer et al. [32] showed that both the direct salt effect (reduction in free volume due to ion exclusion volumes) and the indirect salt effect (modification of water structure and compressibility) contribute approximately equally to the increase in μ^{ex} with salt concentration. For NaCl at 5 mol/L, this increase corresponds to ~10 kJ/mol for a methane-sized cavity [32], a value fully consistent with the magnitude of the increase in cohesive pressure computed in this work.

The critical distinction between Mg^{2+} and Ca^{2+} regarding ion-pair formation can be rationalized through their ionic radii and hydration dynamics [34]. Despite having similar charge (+2) and similar k_i values (2.25 versus 2.10 mN m^{-1} M^{-1} [29]), Mg^{2+} (r = 0.070 nm, Mg–O distance in solution = 0.209 nm [34]) maintains a rigid, highly ordered first hydration shell of six water molecules with exchange rates orders of magnitude slower than those of Ca^{2+} (r = 0.103 nm, Ca–O distance = 0.242 nm [34]). The kinetic persistence of the Mg^{2+} hydration shell, a consequence of its exceptional charge-to-radius ratio, prevents contact ion pair formation with the SDS group under the conditions studied. With its larger radius and more labile hydration shell, Ca^{2+} readily forms such pairs, as evidenced by the destabilization of the foam observed in Regime II. This interpretation is further supported by the surface viscosity data of Pandey et al. [33], which showed that $Mg(DS)_2$ monolayers exhibit approximately 90-fold higher surface viscosity than NaDS monolayers; this is direct evidence that the SDS group retains its full hydration shell and packing efficiency in the presence of Mg^{2+} counter-ions.

2.3.2. The Pitzer Formalism: Decoding Cohesive Pressure in Salt-Laden Domains

The effect of dissolved ionic species on this cohesive pressure can be expressed as follows. By adding the non-ideal osmotic pressure contribution (Π_{osm}), derived from the meticulous Pitzer model [24], onto the baseline cohesion of pure water (Π_0), the following expression is obtained (Equation (3)):

$$\Pi_{coh} = \Pi_0 + \Pi_{osm} \quad (3)$$

This dynamic osmotic contribution is governed by the following expression (Equation (4)):

$$\Pi_{osm} = 1000 \Phi \nu C R T \quad (4)$$

where Φ represents the osmotic coefficient—the mathematical signature of non-ideality—ν is the stoichiometric ion count, C denotes molar concentration, and RT is the product of the

gas constant and absolute temperature. In a pure liquid, Π_{osm} vanishes, yielding a baseline energy density equal to the work required to form a molecular cavity in the pure solvent.

Yet introducing a strongly hydrating "kosmotropic" electrolyte such as $MgCl_2$ significantly alters the thermodynamic properties of the aqueous matrix. The high charge density of these ions causes a substantial restructuring of the solvent network. This is reflected macroscopically in a marked decrease in water activity and a corresponding increase in osmotic pressure. At the molecular level, the energy required to form a cavity for the hydrophobic tail of the surfactant molecule increases substantially beyond simple van der Waals contributions, due to the increased ion-induced restructuring of the water matrix.

When electrolyte concentrations exceed 1.0 mol/dm^3, the elevated osmotic pressure indicates a significant reduction in the availability of free water molecules. Under these conditions, the increased demand for hydration water by the electrolyte raises the energetic barrier to surfactant dispersion. As a consequence, the activity coefficient of SDS increases, promoting its migration to the air/water interface. However, at sufficiently high ionic strengths, this effect is counteracted by ion-specific interactions that can destabilize the adsorbed surfactant film and promote bubble coalescence.

2.3.3. The Energetic Toll of Cavitation and Interface Migration

The energy required to form a cavity of defined volume within the aqueous matrix is given by the following expression (Equation (5)):

$$\frac{\omega_{cav}}{k_B T} = \frac{\Pi_{coh} V_{surf}}{k_B T} \tag{5}$$

where V_{surf} represents the surfactant's partial molar volume [41,42], and $k_B T$ scales this quantity to the thermal energy of a single molecule. The cavitation work determines the adsorption energy of the surface-active ion at the air/water interface [43]:

$$\begin{aligned} \frac{E_{ads}}{k_B T} &= \frac{\omega_{cav}}{k_B T} + \frac{E_{head}}{k_B T} + \frac{\sigma_0 \alpha_0}{k_B T} \\ \frac{\omega_{cav}}{k_B T} &= \frac{u_{CH_2}}{k_B T}(n+1) \end{aligned} \tag{6}$$

Here, $u_{CH_2}/k_B T$ is the dimensionless individual energetic contribution of a single methylene group to the overall adsorption energy of the surfactant molecule, n is the number of carbon atoms in the hydrocarbon chain, $E_{head}/k_B T$ is the dimensionless intrinsic affinity of the hydrophilic headgroup with respect to the bulk water, σ_0 is the baseline surface tension of water, and α_0 represents the spatial footprint of the surfactant molecule at the air/water interface.

The exact value of $u_{CH_2}/k_B T$ is determined by the structure of the adjacent polar headgroup [43]. For SDS, the highly polar sulfate headgroup exhibits a strong adsorption energy of $E_{head}/k_B T = -2.79$ [43] due to its elaborate hydrogen-bonding network with the surrounding water matrix.

Before achieving adsorption, the hydrocarbon tail must perform volumetric work (ω_{cav0}) against this cohesive pressure. By establishing this initial workload in pure water via Equation (6), we can determine the baseline cohesive pressure (Π_0) of the pure solvent (Equation (7)):

$$\Pi_0 = \frac{\omega_{cav0}}{V_{tail}} \tag{7}$$

where V_{tail} ($V_{tail} = 2.46 \times 10^{-4}$ m^3/mol for SDS [41,42]) serves as the volumetric measure of the hydrophobic chain resisting the matrix. Evaluating Equation (7) for the SDS hydrocarbon tail in pure water, with $V_{tail} = 2.45 \times 10^{-4}$ m^3 mol^{-1}, yields a baseline cohesive

pressure of the pure solvent Π_0 = 189.2 MPa. This value is in excellent agreement with the internal water pressure reported by Dack, 150–170 MPa at room temperature, providing independent physical support for the magnitude of the cohesive pressure derived here.

2.3.4. Kosmotropic Anomalies: The Transformation of Polar Groups

When salt is dissolved, the total cohesive pressure (Π_{coh}) of the aqueous solution shifts into its complete, salt-dependent expression (Equation (8)):

$$\Pi_{coh} = \Pi_0 + 1000\Phi\nu CRT \tag{8}$$

Utilizing Pitzer's virial coefficients [24] to evaluate the osmotic contribution. At high ionic strengths, kosmotropic electrolytes (such as $MgCl_2$ and NaCl) immobilize a significant fraction of water molecules within their hydration shells, partitioning the solvent matrix into two distinct domains:

(i). rigidly bound, structured hydration complexes;
(ii). transient pockets of free water.

This partitioning increases the effective cohesive pressure of the solution, raising the cavitation work ω_{cav}/k_BT by a factor (ξ) (Equation (9)):

$$\begin{gathered} \xi = \frac{\Pi_0+\Pi_{osm}}{\Pi_0} = \frac{\Pi_{coh}}{\Pi_0} \\ \frac{\omega_{cav}}{k_BT} = \xi\frac{u_{CH_2}^{(salt)}}{k_BT}(n+1) \end{gathered} \tag{9}$$

A further consequence of strong kosmotropic conditions is the alteration of the chemical character of the surfactant headgroup itself. Under high ionic strength, the high hydration energy of Mg^{2+} ions progressively displaces water molecules from the SDS headgroup. The same applies to all cosmotropic ions. Progressive dehydration of the sulfate headgroup effectively converts it from a hydrophilic to a hydrophobic moiety. It should be stressed that this scenario describes a limiting, end-member case of extreme head-group dehydration. It is invoked here only to define the upper bound of the cavitation-volume effect and is not realized for the strongly hydrated, kinetically inert Mg^{2+} ion, whose hydration shell is preserved under all conditions studied (see below); for Mg^{2+} the relevant role is the preservation of head-group hydration, not its dehydration. As a result, the effective cavitation volume of the SDS molecule increases, modifying the required cavity dimensions. The adsorption energy of the dehydrated headgroup can be expressed through the following volumetric ratio (Equation (10)):

$$\frac{u_{SO_4^-}}{k_BT} = \frac{u_{CH_2}^{(salt)}}{k_BT}\frac{V_{SO_4^-}}{V_{CH_2}} \tag{10}$$

With V_{head} = 45 cm^3/mol and V_{CH2} = 27 cm^3/mol [41], the total work required to accommodate this modified molecule under intense ionic strength becomes (Equation (11)):

$$\frac{\omega_{cav}^{(salt)}}{k_BT} = \frac{u_{CH_2}^{(salt)}}{k_BT}(n+3) \tag{11}$$

From this complex cavitation workload, we can deduce the final structural volumes and interfacial energies driving the system:

$$V_{surf}^{(salt)} = \frac{\omega_{cav}^{(salt)}}{\Pi_{coh}} \tag{12}$$

$$\frac{E_{ads}}{k_B T} = \frac{\omega_{cav}^{(salt)}}{k_B T} + \frac{\sigma_0 \alpha_0}{k_B T} \tag{13}$$

where σ_0 represents the surface tension of the electrolyte solution. This result indicates a notable difference from the baseline case: the contribution of the hydrophilic head (Equation (6)) is absent from Equation (13). Stripped of its water shield by the competitive pull of Mg^{2+} ions, the sulfate group loses its hydrophilic character and contributes to the overall hydrophobic volume of the molecule, thereby increasing the effective interfacial driving force for SDS adsorption at the air/water interface. The relation between the adsorption energy and the equilibrium adsorption constant K of the ionic surfactants is as follows [43–46]:

$$\begin{aligned} K_s &= \delta_s \exp\left(\tfrac{E_{ads}}{k_B T}\right) \\ K_0 &= \left(\tfrac{4K_s}{\kappa_0^2}\right)^{\frac{1}{3}} \\ \ln K &= \ln K_0 - \tfrac{1}{2}\tfrac{u_0}{k_B T} \end{aligned} \tag{14}$$

where K_s is the adsorption constant of the surfactant molecule with excluded charge (non-ionic form), K_0 is the adsorption constant of the surface-active ion (with included charge) but excluded adsorption of its counter-ion on the air/water interface and K is the real equilibrium adsorption constant of the ionic surfactant, i.e., with included adsorption of the counter-ion with specific adsorption energy $u_0/k_B T$, which can be calculated additionally [41,47], $\delta_s = l_{CH_2}/\frac{u_{CH_2}}{k_B T}$ is adsorption length, $l_{CH_2} = 0.126$ nm is the length of one CH_2 group, $u_{CH_2}/k_B T$ is the dimensionless adsorption energy of one methylene group, $\kappa_0^2 = 8\pi e^2/\varepsilon k_B T$, e is the charge of electron (in CGS system), k_B is the Boltzmann constant (in CGS system), ε is dielectric permittivity of water and T is absolute temperature.

2.3.5. Interfacial Activities and Setchenov Scaling Realities

The effective activity of the surfactant within this altered landscape scales in accordance with the classical Setchenov relation:

$$\begin{aligned} a_{surf} &= C_{surf} f_{surf} \\ f_{surf} &= \exp(K_s m_{salt}) \end{aligned} \tag{15}$$

where a signifies the overall activity, K_s is the characteristic Setchenov parameter, and m_{salt} represents the molality of the salt. The empirical constants governing these interactions are detailed below in Table 1 [31,42,43]:

Table 1. Electrolytes studied in this work, their Setschenow constant, and their corresponding salting-out effects on organic molecules.

Electrolyte	Setschenow Constant Ks, m^{-1}	Effect Character
NaCl	0.20	Moderate salting-out
KCl	0.15	Weak salting-out
$MgCl_2$	0.40	Strong salting-out
$CaCl_2$	0.33	Strong salting-out

In highly concentrated regimes of cosmotropic salts, the activity coefficient of the surfactant increases substantially due to the significant decrease in the availability of free water. By employing the Pitzer model [24] alongside established virial coefficients ($\beta 0$, $\beta 1$, and C), we can accurately trace these mean ionic activities and osmotic functions (φ), identifying the boundaries of phase separation.

3. Results

Our experimental analysis begins by considering the foam reactor as a dynamic system consisting of two distinct zones: the bubble emulsion (bulk) and the foam layer. The stability of the foam layer is depends on the conditions established in the bubble emulsion zone. We observed that the transition from a stable to unstable foam is largely influenced by the background electrolyte composition. This interaction is not limited to the surfactant alone but fundamentally alters the water matrix.

3.1. Thermodynamic Mechanism of Salt–Frother Interaction

To explain the experimental observations, we apply the Pitzer theory [24], which takes into account the non-ideal behavior in concentrated electrolyte solutions. Our data indicates that salt ions interact with water molecules, significantly increasing the cohesive pressure of the water network. At low electrolyte concentrations, the predominant mechanism is the screening of electrostatic repulsion between the anionic head groups (DS^-) of SDS molecules. This screening effect facilitates the adsorption of SDS at the air–water interface. However, at higher concentrations, the mechanism shifts. As the salt concentration increases, the surfactant molecule must expend more energy to create a "cavity" within the water matrix against this increased cohesive pressure. Consequently, the frother's activity coefficient increases, thereby enhancing its adsorption. Figure 2 shows the osmotic and activity coefficients of the electrolytes studied: (A) and (B) show the trends for $CaCl_2$ and $MgCl_2$, while (C) and (D) represent the data for NaCl and KCl. These coefficients confirm that the non-ideal behavior of the system, particularly at high molarities, is directly proportional to the ion-specific hydration properties of the chosen salts. The observed divergence in these coefficients aligns with our theoretical hypothesis, suggesting that $MgCl_2$ and $CaCl_2$ exert a much stronger influence on the water structure than monovalent salts, thereby directly affecting the energy barrier for bubble coalescence.

3.2. Ion-Specific Effects and Collins' Rule of Matching Water Affinities

Our experimental results demonstrate that the stability of SDS foam is not determined solely by electrostatic screening, but is fundamentally governed by the hydration compatibility between surfactant head groups and salt ions. To interpret the observed variations in electrolyte behavior, we apply Collins' Rule of Matching Water Affinities [21], which suggests that the interaction strength between ions is maximized when their hydration energies are similar. The broader implications of ion-specific effects on soft matter systems, including the behavior of chaotropic ions beyond the standard lyotropic series and their interactions with surfactant aggregates, have been reviewed by Leontidis [48]. Our data confirm that the stabilization mechanism shifts according to the dehydration energy of the ion:

$MgCl_2$–SDS (Strong Kosmotrope–Weak Kosmotrope): Magnesium ions are strongly hydrated ("hard" ions) and compatible with the high water affinity of the SDS head groups. Maintaining this hydration shell prevents the formation of direct-contact ion pairs (CIPs), thereby ensuring maximum foam stability.

$CaCl_2$ (Kosmotrope–Weak Kosmotrope): The dehydration energy of calcium ions is lower than that of magnesium. This energetic profile allows them to "match" and form stable contact ion pairs by directly binding to SDS head groups. This process neutralizes the surface charge and collapses the protective water film, which explains the rapid coalescence observed in our experiments.

NaCl (Strong Kosmotrope) and KCl (Chaotrope): These ions follow the same fundamental principle but exert lower cohesive pressure, resulting in moderate to low stabilization effects depending on their specific positions in the Hofmeister series. These

interactions are summarized in Table 2, which correlates the ion properties with the resulting foam stability.

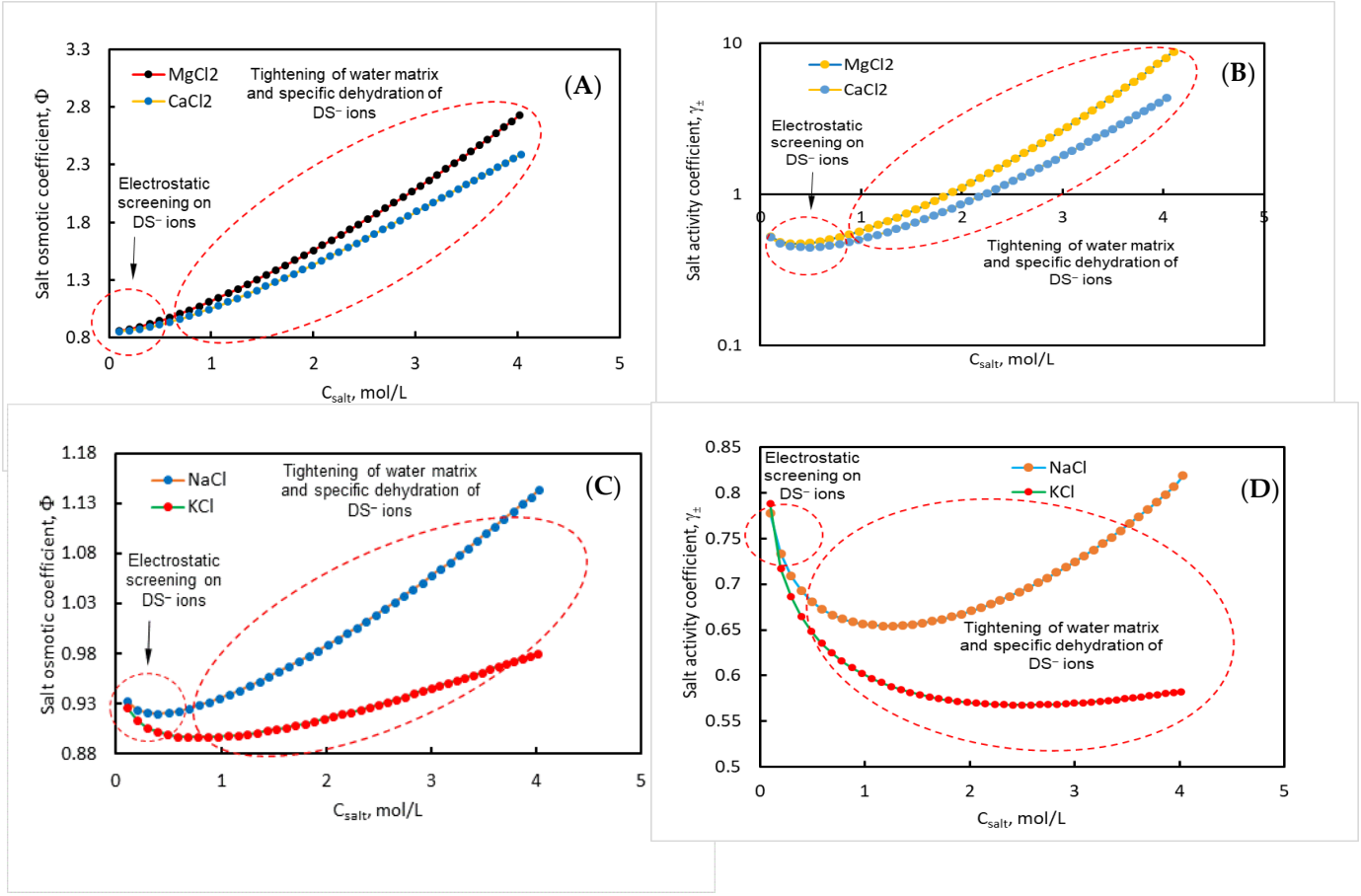

Figure 2. Osmotic and activity coefficients for: (**A**,**B**)—$CaCl_2$ and $MgCl_2$; (**C**,**D**)—NaCl and KCl.

Table 2. CCC values of NaCl, KCl, SDS, and SDS in the presence of each salt at their CCC values.

	NaCl	*KCl*	*SDS*	*SDS at CCC (NaCl)*	*SDS at CCC (KCl)*
CCC, mol/dm^3	0.2	0.3	6×10^{-6}	3×10^{-7}	4×10^{-7}

3.3. Effect of Salts on the Air/Water Interface in the Presence of SDS

Adding electrolytes to an aqueous SDS solution significantly alters the state of the air/water interface. This effect can be divided into two distinct concentration-dependent regimes, as demonstrated by our surface tension measurements and theoretical analysis. A basic proxy of the state of the air/water interface is the surface tension value, which usually reflects the difference between the standard chemical potentials of the water molecules at the water/air interface and the standard chemical potentials of the water molecules in the bulk [49]:

$$\sigma = \frac{\mu_0^s - \mu_0^b}{\omega} \quad (16)$$

where μ_0^s and μ_0^b are the standard chemical potentials of water molecules at the air/water interface and in the bulk, respectively, and ω is the cross-sectional area per water molecule at the air/water interface.

As seen in Figure 3, the surface tension (σ) of the SDS solution (5×10^{-5} mol/dm^3) exhibits a non-linear dependence on the concentration of the added electrolytes. This

dependence clearly distinguishes two concentration-dependent regimes, which can be interpreted in termsof surface charge screening and bulk-driven adsorption.

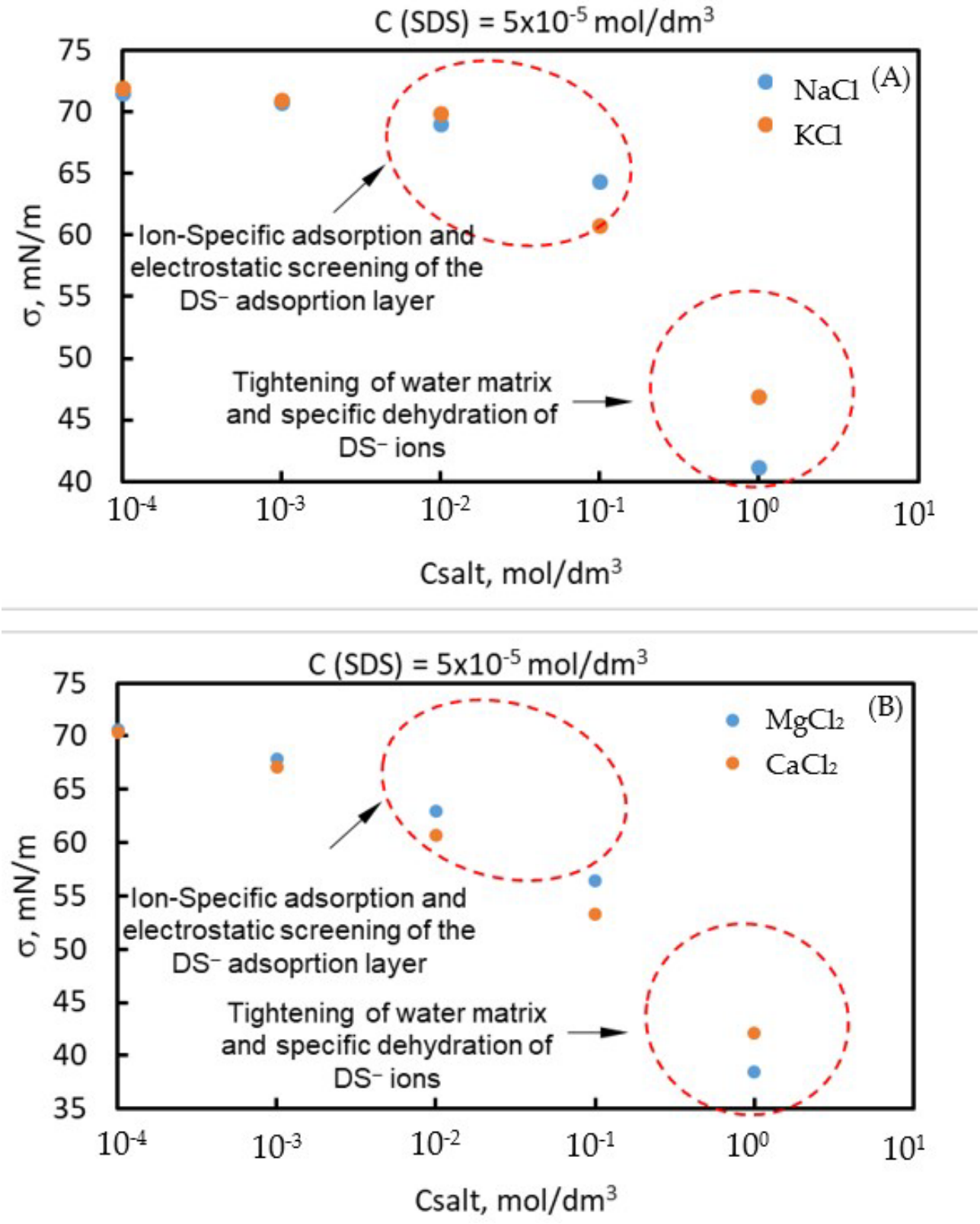

Figure 3. Surface tension of 5×10^{-5} mol/dm^3 SDS versus concentration of added salt: (**A**) NaCl and KCl; (**B**) $MgCl_2$ and $CaCl_2$. Measurements were performed at room temperature; salt concentrations are given in mol dm^{-3}. Error bars correspond to the instrumental reproducibility of the surface-tension measurement ($\pm$0.3 mN m^{-1}).

3.3.1. Regime I: Low Salt Concentration (Electrostatic Screening)

At low electrolyte concentrations (C_{salt} < 0.2 mol/dm^3), all the salts investigated (NaCl, KCl, $MgCl_2$, and $CaCl_2$) cause a sharp decrease in surface tension. In this regime, the primary role of the salt is to provide counter-ions that screen the electrostatic repulsion between the adsorbed anionic DS^- head groups. According to the classic view proposed by Alty [50], the interface acts as a region where selective ion adsorption occurs. The presence of Na^+, K^+, Mg^{2+}, or Ca^{2+} ions increases the "surface capacity" for surfactant molecules, allowing for a more densely packed adsorption layer. The standard chemical potential of the water molecules at the interface (μ_0^s) decreases as they are replaced or reorganized by the increased presence of surfactant and screening ions. This leads to a significant decrease in σ (as per Equation (3)), effectively boosting the foam stability in the initial stages.

Another well-known proxy of the state of the air/water interface is the fraction of bubble coalescence and the related critical coalescence concentration (CCC, 50% fraction of bubble coalescence) of the frothers. The salts used in this work have their own CCC values because they reduce the fraction of bubble coalescence. This is a well-known salt effect, reflected in the literature [48–53], and explained by the slowing of bubble–bubble collisions due to the specific action of the salt. This kinetic effect arises from the unequal concentration profiles of salt anions and cations at the air/water interface and causes an electrokinetic streaming potential that slows the thinning of the foam films between bubbles during their collision [47]. Figure 4 shows the bubble fraction coalescence as a function of: (i) salts added in surfactant-free solution; (ii) SDS concentration in salt-free solution and at the CCC values of the salts studied.

The bubble fraction coalescence decreases with increasing the concentration of each particular salt and SDS. As expected, the effect of the surfactant on bubble coalescence inhibition is much stronger than that of each salt alone. The CCC values for each particular case are presented in Tables 2 and 3. In each salt pair (NaCl and KCl; $MgCl_2$ and $CaCl_2$), the CCC values are close to each other, and only the charge of the ions is significant. This indicates a lack of salt specificity in these diluted salt solutions. Evidently, the electrostatic screening is the dominant effect here.

Table 3. CCC values of $MgCl_2$, $CaCl_2$, SDS and SDS at the CCC values of each particular salt.

	MgCl₂	***CaCl₂***	***SDS***	***SDS at CCC (MgCl₂)***	***SDS at CCC (CaCl₂)***
CCC, mol/dm^3	0.01	0.07	6×10^{-6}	5×10^{-7}	3×10^{-7}

Moreover, as can be seen in Figure 5, the CCC value of SDS at the specified salt concentrations is almost identical to that of pure water. Secondly, it is noted that the fraction of bubble coalescence is a significantly more sensitive proxy to the state of the air/water interface than the surface tension value.

3.3.2. Regime II: High Salt Concentration—The Divergence of Stability and the Role of Cohesive Pressure

When the electrolyte concentration increases far beyond 0.1 mol/dm^3, the system enters Regime II; in this regime, the behavior of the gas emulsion and the resulting foam is no longer governed solely by electrostatic screening. In this regime, despite similar surface tension values, we observe a significant divergence in foam stability between different salts. This phenomenon can be explained by integrating Pitzer's thermodynamic framework [24] with Collins' Concept of Matching Water Affinities [21]. Figure 6 shows how the foam height for 5×10^{-5} mol/dm^3 SDS, either alone or in the presence of 1 mol/dm^3 added salt, depends on time during the regimes of foam growth and foam decay. As can be seen

in Figure 6A, 1 mol/dm^3 NaCl significantly increases the foam, while 1 mol/dm^3 KCl results in a complete lack of foamability. Similarly, Figure 6B shows that 1 mol/dm^3 $MgCl_2$ boosts the foam identically to NaCl, whereas 1 mol/dm^3 $CaCl_2$ acts as a weaker defoamer than KCl. A more precise presentation of these effects is shown in Figure 7, which shows the dynamic foam stability (Bikerman foaminess [54]) of 5 × 10^{-5} mol/dm^3 SDS versus the concentration of the added salt. One can see that NaCl and KCl affect the foaminess similarly up to 0.1 mol/dm^3, but above this concentration, KCl acts as a defoamer, whereas NaCl acts as a foam booster. The same is valid for the $MgCl_2$ and $CaCl_2$ pair, but the concentration borderline is two orders of magnitude less–1 × 10^{-3} mol/dm^3.

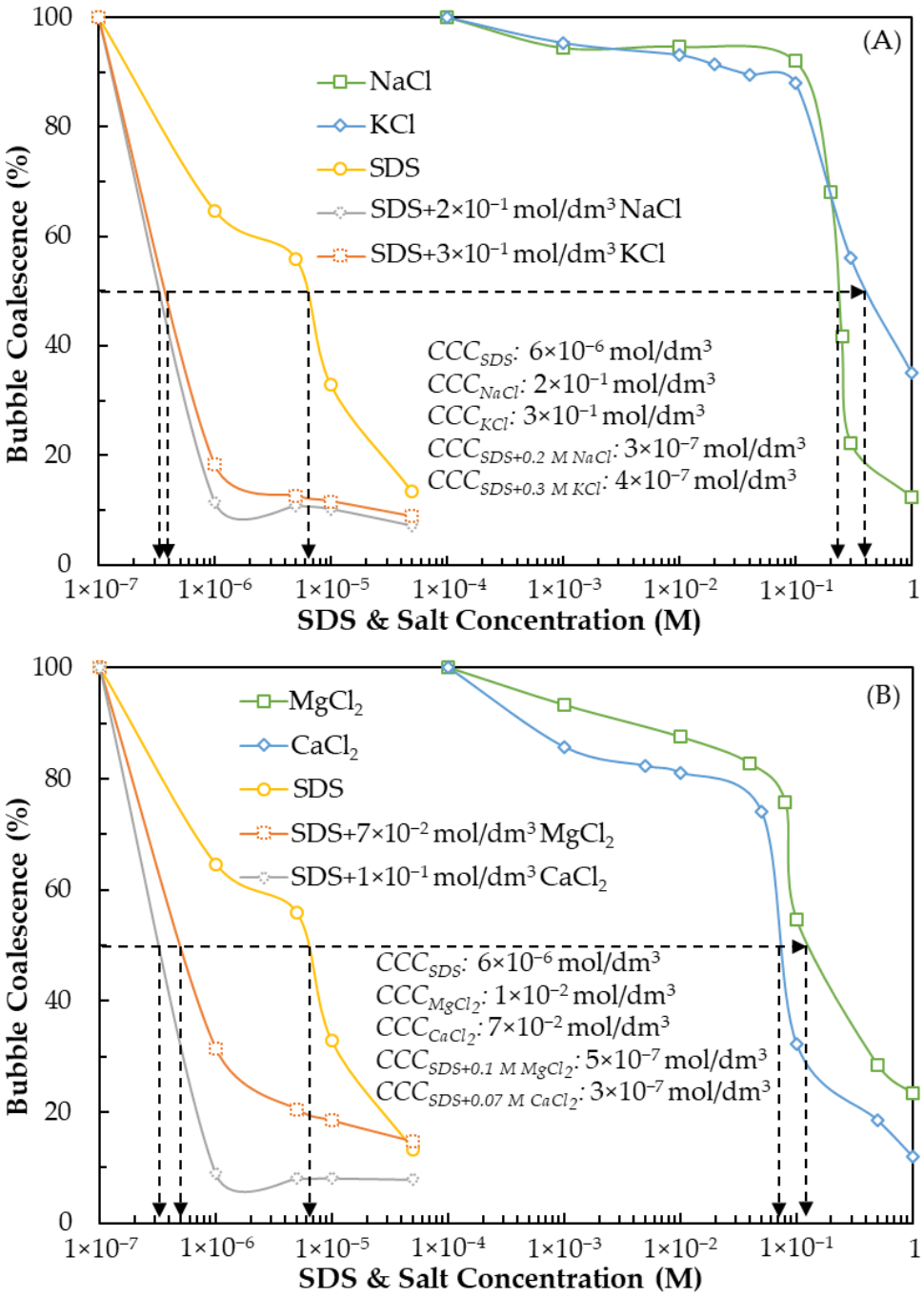

Figure 4. Fraction of the bubble coalescence versus: (**A**) (i) concentration of NaCl and KCl in surfactant-free solution; (ii) concentration of SDS in salt-free solution and in the presence of NaCl and KCl at their CCC; (**B**) (i) concentration of $MgCl_2$ and $CaCl_2$ in surfactant = free solution; (ii) concentration of SDS in salt-free solution and in the presence of $MgCl_2$ and $CaCl_2$ at their CCC.

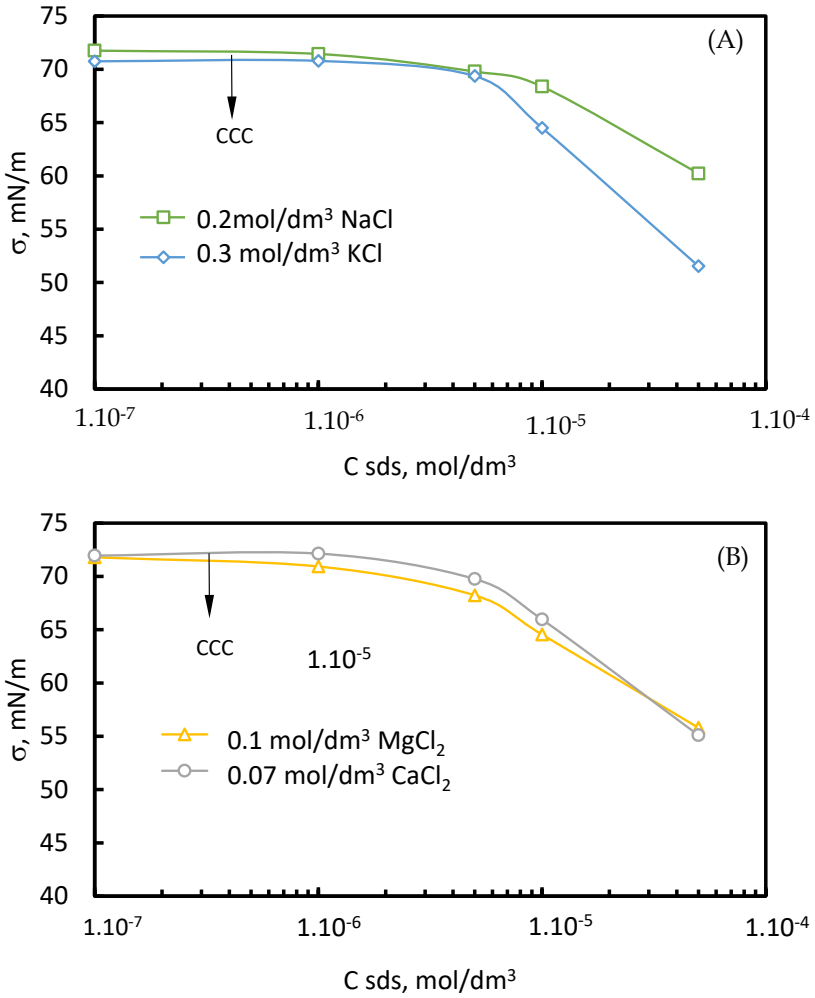

Figure 5. Surface tension isotherms of SDS at: (**A**) 0.2 mol/dm^3 NaCl and 0.3 mol/dm^3 KCl; (**B**) 0.1 mol/dm^3 $MgCl_2$ and 0.07 mol/dm^3 $CaCl_2$.

1. The Driving Force: Cohesive Pressure (Pitzer Approach) [24]

At high concentrations, the salt significantly modifies the bulk properties of the water matrix. According to the Pitzer model [24], the presence of ions increases the osmotic coefficient and the activity of water, which macroscopically manifests as an increase in the cohesive pressure (Π_{coh}) of the solution. Theoretically, a higher Π_{coh} increases the energy cost of maintaining a cavity in the liquid (ω_{cav}). To minimize this energy, the hydrophobic tails of the SDS molecules are more effectively "squeezed out" toward the air/water interface. This explains why $MgCl_2$ and NaCl act as "foam boosters" in this regime; the reinforced water structure forces a denser surfactant packing, strengthening the film.

2. The Stability Judge: Hydration Matching (Collins' Rule) [21]

The collapse of foam observed at high $CaCl_2$ concentrations, when compared to the stability of $MgCl_2$, reveals the decisive role of ion-specific hydration:

The Mg^{2+} Case (Strong Hydration): Magnesium is a strong "kosmotrope" with a very high dehydration energy. It retains its hydration shell even when crowded at the interface. This prevents direct contact with the SO_4^- heads of SDS, maintaining a stable, hydrated liquid film between the bubbles that resists coalescence.

The Ca^{2+} Case (Ion-Pair Formation): Calcium has a lower dehydration energy than magnesium. In Regime II, the high concentration forces Ca^{2+} to "match" the hydration

affinity of the SDS head groups. This situation leads to the formation of Contact Ion Pairs (CIP). The formation of these pairs effectively neutralizes the surface charge and eliminates the protective hydration layer, leading to immediate film rupture and bubble coalescence.

3. Conclusion of the Dual-Regime Model

The transition from Regime I to Regime II marks a shift from Alty's [50] surface charging to Pitzer's bulk thermodynamics and Collins' molecular specificity. Surface tension (Figure 3) indicates the interface state, while the coalescence fraction (Figure 4) is the true indicator of the competitive forces between cohesive pressure (stabilizing) and ion-pair formation (destabilizing).

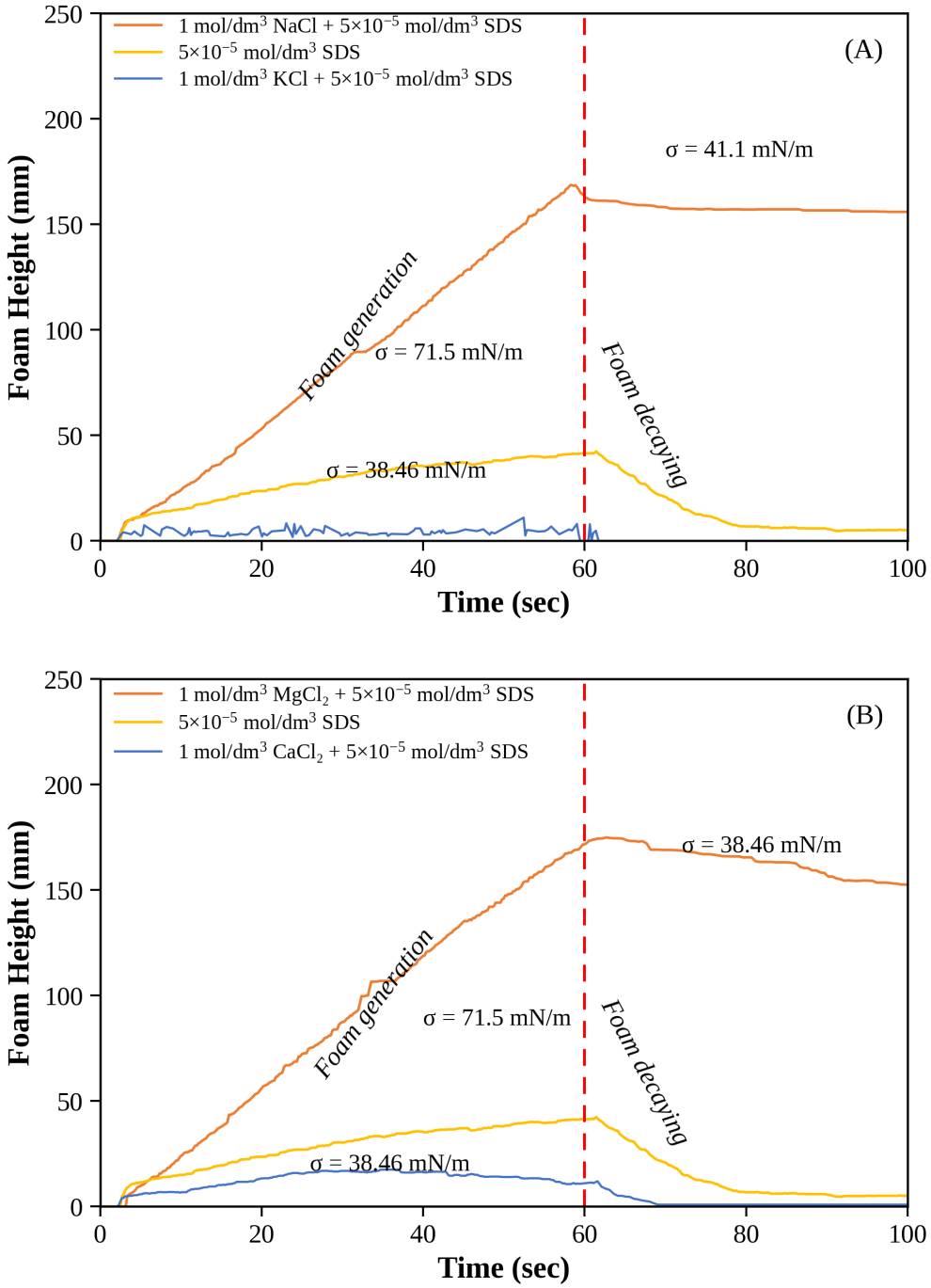

Figure 6. Foam height versus time of: (**A**) 5×10^{-5} mol/dm^3 SDS + 1 mol/dm^3 NaCl, 5×10^{-5} mol/dm^3 SDS; 5×10^{-5} mol/dm^3 SDS + 1 mol/dm^3 KCl; (**B**) 5×10^{-5} mol/dm^3 SDS + 1 mol/dm^3 $MgCl_2$, 5×10^{-5} mol/dm^3 SDS; 5×10^{-5} mol/dm^3 SDS + 1 mol/dm^3 $CaCl_2$.

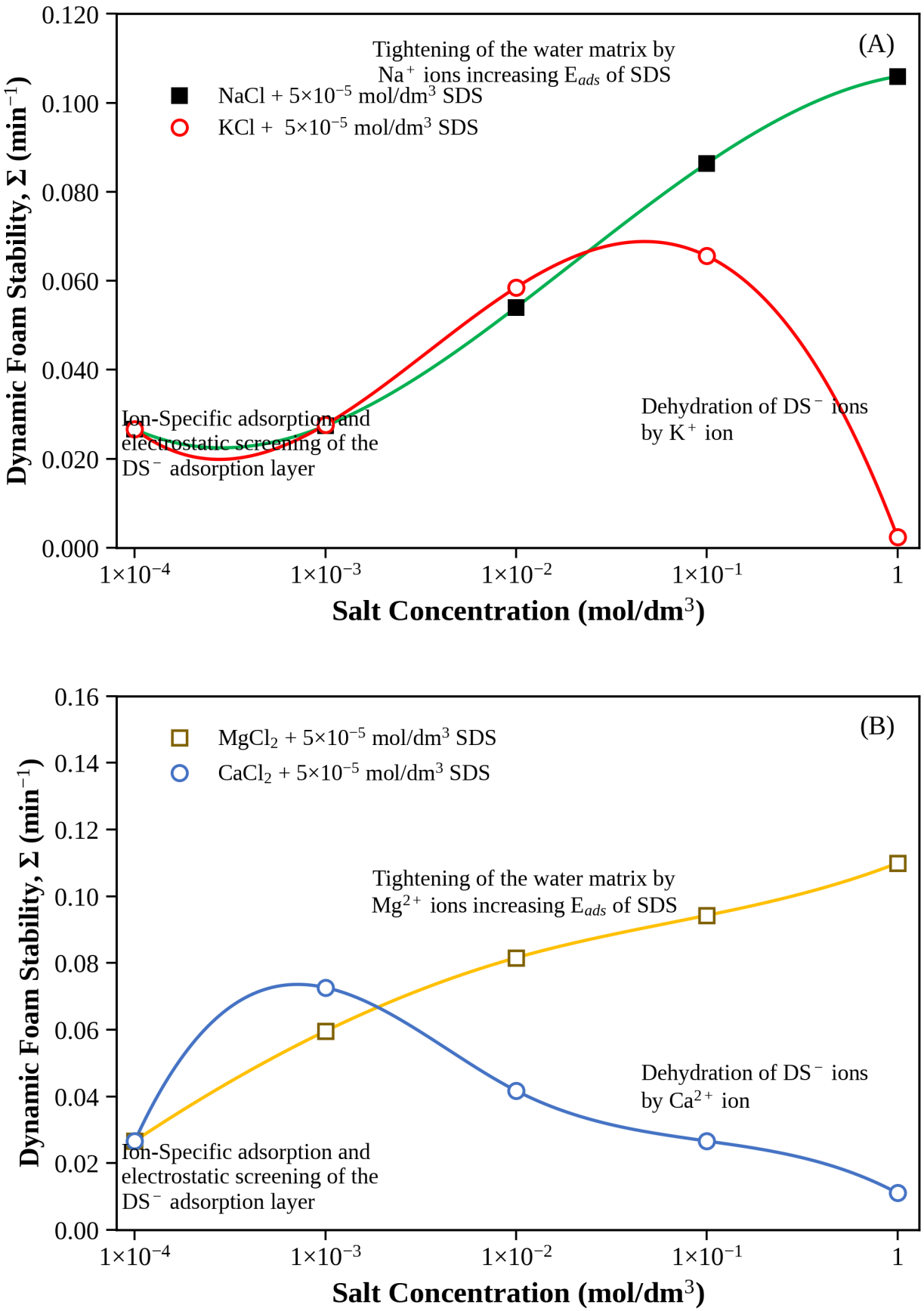

Figure 7. Dynamic Foam Stability versus salt concentration of: (**A**) 5×10^{-5} mol/dm^3 SDS + NaCl, 5×10^{-5} mol/dm^3 SDS + KCl; 5×10^{-5} mol/dm^3 SDS + 1 mol/dm^3 KCl; (**B**) 5×10^{-5} mol/dm^3 SDS + $MgCl_2$, 5×10^{-5} mol/dm^3 SDS + $CaCl_2$.

4. Discussion

The experimental results presented in this work reveal a clear bifurcation in the response of SDS foam stability to added electrolytes at concentrations above 0.1 mol/dm^3. While all four salts (NaCl, KCl, $MgCl_2$, and $CaCl_2$) produce nearly identical effects at low concentrations (consistent with a dominant electrostatic screening mechanism) their behavior diverges sharply in Regime II, where ion-specific interactions govern the outcome. This divergence cannot be rationalized by the classical DLVO theory alone and requires a framework that explicitly accounts for the kinetics of ion hydration and the thermodynamic state of the bulk solvent.

The observed ion-specific behavior can be conceptually unified through a kinetic–thermodynamic framework based on a mechanistic weighting coefficient α, which quantifies the propensity of a given cation to form contact ion pairs (CIPs) with the DS^- head group of SDS. This coefficient is defined by the ratio of a reference diffusional encounter time τ_{enc} to the effective water-exchange residence time τ_{enc} of the cation's first hydration shell:

$$\alpha_i(C) = \frac{\tau_{enc}}{\tau_i^{eff}(C) + \tau_{enc}} \tag{17}$$

where the effective residence time $\tau_i^{eff}(C)$ increases with salt concentration through the cohesive pressure magnification factor $\xi(C) = \Pi_{coh}(C)/\Pi_0$, which is directly calculable from the Pitzer formalism developed in Section 2.3. Physically, α_i represents the probability that a given cation successfully dehydrates sufficiently during a diffusional encounter with DS^- to form a contact ion pair. When $\alpha \to 1$, the chemical pathway dominates (ion-pairing and surfactant precipitation); when $\alpha \to 0$, the physicochemical pathway dominates (cohesive pressure enhancement and foam stabilization). It should be emphasised that α_i is introduced here as a conceptual, semi-quantitative descriptor that organises the observed ion-specific trends along a single kinetic–thermodynamic axis, rather than as a fully validated predictive model; a complete tri-component summation $\Sigma(C)$ capable of quantitative prediction is reserved for future work. In particular, α_i measures only the propensity of a cation to access the chemical (ion-pairing) pathway and does not by itself determine the sign of the net effect on foam stability. The observed outcome reflects the competition between this propensity (α) and the cohesive-pressure enhancement (ξ): a rapidly exchanging cation such as Na^+ has a high α, yet at the concentrations studied here, the cohesive-pressure contribution dominates, so the net effect of NaCl is foam-boosting. Thus, a high value of α is not in contradiction with the foam-stabilising behaviour of NaCl.

The values of α_i computed for all studied cations, using experimentally determined water-exchange residence times from NMR measurements [54] and the Pitzer-derived cohesive pressures from this work, are summarized in Table 4. The residence times span nearly ten orders of magnitude: K^+ ($\tau_0 \approx 4$ ps) and Na^+ ($\tau_0 \approx 14$ ps) exchange water rapidly, yielding $\alpha \approx 0.99$ at all studied concentrations. In stark contrast, Mg^{2+} ($\tau_0 \approx 2 \times 10^6$ ps) maintains a rigid, inert hydration shell, giving $\alpha \approx 0$ throughout. Ca^{2+} ($\tau_0 \approx 110$ ps) occupies the transitional zone, with $\alpha \approx 0.90$ at low concentrations, decreasing significantly at concentrations above 2 mol/dm^3 as the elevated cohesive pressure progressively immobilizes its hydration shell.

The internal consistency of this descriptor is illustrated by comparing it with our study [37], investigating the defoaming effect of LiCl, NaCl, and KCl on SDS foams. In that work, it was determined that KCl was the most potent defoamer, acting via a chemical pathway (specific ion-pairing leading to surfactant precipitation), while LiCl and NaCl operated through a physicochemical pathway (massive increase in bulk cohesive pressure). The present framework is consistent with this ordering: K^+ ($\alpha \approx 0.996$) and Na^+ ($\alpha \approx 0.986$) are classified as chemical-pathway ions, while the high cohesive pressure of concentrated

LiCl solutions ($\xi \approx 1.18$ at 4 mol/dm^3) drives $\alpha(Li^+)$ toward zero at extreme concentrations, consistent with the observed physicochemical defoaming mechanism. The present work extends this picture to divalent cations: Mg^{2+} ($\alpha \approx 0$) acts as a pure physicochemical stabilizer through cohesive pressure enhancement, while Ca^{2+} ($\alpha \approx 0.90$ at low C, decreasing at high C) straddles the mechanistic boundary, exhibiting defoaming behavior that is weaker than KCl but more pronounced than that of NaCl at equivalent concentrations. This behavior is consistent with Ca^{2+}'s intermediate water-exchange kinetics ($\tau_0 \approx 110$ ps), which permit partial contact ion-pair formation without the full dehydration characteristic of K^+. Therefore, the critical distinction between Ca^{2+} and Mg^{2+} lies not in their charge or thermodynamic hydration free energies per se, but in the kinetic lability of their respective hydration shells; this finding extends and refines the original Collins' Rule by introducing an explicit kinetic dimension.

Table 4. Mechanistic weighting coefficient α_i for the studied cations at selected salt concentrations ($C_{SDS} = 5 \times 10^{-5}$ mol/dm^3). τ_0 values from ref. [54]; $\xi(C)$ calculated from the Pitzer model (this work).

Cation	τ_0 (ps)	n_{hyd}	α (0.1 M)	α (1.0 M)	Dominant Mechanism	Obs.
K^+	4.1	6	0.996	0.995	Chemical (SIP)	$\uparrow \Sigma$
Na^+	14.1	6	0.986	0.983	Chemical (weak)	$\uparrow \Sigma$
Ca^{2+}	110	8	0.898	0.853	Transitional ($\alpha \downarrow$ at high C)	$\uparrow \Sigma$
Mg^{2+}	2×10^6	6	0.0005	0.0003	Physico-chemical	$\uparrow \Sigma$

5. Conclusions

This study investigated the ion-specific effects of NaCl, KCl, $MgCl_2$, and $CaCl_2$ on the dynamic foam stability (Σ) of dilute SDS solutions (5×10^{-5} mol/dm^3) over a wide range of electrolyte concentration (10^{-4}–1 mol/dm^3). The main conclusions are as follows:

1. Two concentration-dependent regimes govern foam stability. In Regime I ($C < 0.1$ mol/dm^3), all four salts act identically through electrostatic screening of the DS^- head groups, reducing bubble coalescence and enhancing foam stability. Ion specificity is absent at this stage: the critical coalescence concentration (CCC) values within each valence pair (NaCl/KCl; $MgCl_2$/$CaCl_2$) are nearly equal, confirming that ionic charge, not identity, controls the outcome.
2. In Regime II ($C > 0.1$ mol/dm^3), pronounced ion-specific divergence emerges. $MgCl_2$ and NaCl act as foam stabilizers (Σ increases monotonically), while KCl and $CaCl_2$ act as defoamers (Σ peaks then collapses). The divergence onset for the divalent pair is two orders of magnitude lower in concentration than for the monovalent pair, reflecting the much greater cohesive pressure generated by divalent ions.
3. The Pitzer thermodynamic model quantitatively describes the bulk non-ideality of each salt solution through the cohesive pressure parameter Π_{coh} and the dimensionless ratio $\xi = \Pi_{coh}/\Pi_0$. The cohesive pressure increases monotonically with concentration for all salts, and is substantially larger for $MgCl_2$ and $CaCl_2$ than for the monovalent chlorides at equivalent molarity. This increase in cohesive pressure drives enhanced SDS adsorption at the air/water interface through cavity formation thermodynamics, providing the physical basis for foam stabilization in Regime II.
4. The foam destabilization observed with KCl and $CaCl_2$ is interpreted through Collins' Rule of Matching Water Affinities. K^+ and Ca^{2+} possess water-exchange kinetics fast enough to partially dehydrate during diffusional encounters with the DS^- head group, forming contact ion pairs (CIPs) that neutralize surface charge and rupture the

foam film. In contrast, Mg^{2+} retains its hydration shell under all studied conditions, preventing CIP formation and maintaining foam stability. Na^+, despite its chemical classification as a CIP-forming ion, generates sufficient cohesive pressure at high concentrations to stabilize the foam through the physicochemical pathway.

5. Ca^{2+} occupies a transitional position between the two mechanistic extremes. Its intermediate water-exchange residence time ($\tau_0 \approx 110$ ps, compared to $\tau_0 \approx 4$ ps for K^+ and $\tau_0 \approx 2 \times 10^6$ ps for Mg^{2+}) permits partial CIP formation while simultaneously generating significant cohesive pressure. The net result is a weaker defoaming effect than that of KCl, consistent with experimental observations. This finding demonstrates that the chemical/physicochemical mechanical boundary is controlled by hydration shell kinetics, not thermodynamic hydration free energy alone—a refinement of the original Collins' Rule.
6. A mechanistic weighting coefficient $\alpha_i(C)$ is proposed to quantify the fraction of defoaming activity attributable to the chemical (CIP-formation) pathway. Values near unity (K^+: $\alpha = 0.996$; Na^+: $\alpha = 0.986$) indicate a high propensity to access the chemical pathway, while values near zero (Mg^{2+}: $\alpha \approx 0$) indicate a dominant physicochemical character. Ca^{2+} ($\alpha \approx 0.90$ at low C, decreasing at high C) lies in the transitional zone. The coefficient measures propensity only and does not, by itself, determine the sign of the net effect on foam stability; for Na^+, the cohesive-pressure contribution outweighs the ion-pairing propensity, so NaCl is net foam-boosting. This coefficient, derived from Pitzer cohesive pressures and literature NMR water-exchange times [54], provides a conceptual, semi-quantitative descriptor for ion-specific foam behavior that is consistent with results from our companion study on LiCl/NaCl/KCl systems [37].

Author Contributions: Conceptualization, S.I.K. and O.O.; methodology, Y.E.Ç.; software, N.A.G. and K.M.; validation, S.I.K., O.O. and C.C.; formal analysis, D.I.-S.; investigation, S.D., N.A.G. and K.M.; resources; data curation, S.I.K.; writing, S.I.K., visualization, I.Y. and T.T.; supervision, S.I.K. and O.O.; project, S.I.K. and C.C.; funding acquisition, S.I.K. and D.I.-S. All authors have read and agreed to the published version of the manuscript.

Funding: This research was funded by European Union-NextGenerationEU, through the National Recovery and Resilience Plan of the Republic of Bulgaria, project No. BG-RRP-2.013-0001 and project РД-08-84/02.02.2026 of the University of Shumen.

Data Availability Statement: The original contributions presented in this study are included in the article. Further inquiries can be directed to the corresponding authors.

Conflicts of Interest: The authors declare no conflicts of interest.

References

1. Nguyen, A.V.; Schulze, H.J. *Colloidal Science of Flotation*; Marcel Dekker: New York, NY, USA, 2004; p. 840.
2. Janczuk, B.; Bruque, J.M.; Gonzalez-Martin, M.L.; Roman-Galan, E. The contribution of double layers to the free energy of interactions in the cassiterite-SDS solution system. *Colloids Surf. A* **1995**, *100*, 93–103. [CrossRef]
3. Hines, J.D.; Fragneto, G.; Thomas, R.K.; Garrett, P.R.; Rennie, G.K.; Rennie, A.R. Neutron Reflection from Mixtures of Sodium Dodecyl Sulfate and Dodecyl Betaine Adsorbed at the Hydrophobic Solid/Aqueous Interface. *J. Colloid Interface Sci.* **1997**, *189*, 259–267. [CrossRef]
4. Warszynski, P.; Barzyk, W.; Lunkenheimer, K.; Fruhner, H. Surface Tension and Surface Potential of Na n-Dodecyl Sulfate at the Air-Solution Interface: Model and Experiment. *J. Phys. Chem. B* **1998**, *102*, 10948–10957.
5. Lu, J.; Thomas, R.; Penfold, J. Surfactant layers at the air/water interface: Structure and composition. *Adv. Colloid Interface Sci.* **2000**, *84*, 143–304. [CrossRef] [PubMed]
6. Maiti, K.; Mitra, D.; Guha, S.; Moulik, S.P. Salt effect on self-aggregation of sodium dodecylsulfate (SDS) and tetradecyltrimethylammonium bromide (TTAB): Physicochemical correlation and assessment in the light of Hofmeister (lyotropic) effect. *J. Mol. Liq.* **2009**, *146*, 44–51. [CrossRef]

7. Li, K.; Zhang, J.; Li, Q. Study on Foaming Properties of Sodium Dodecyl Sulfate for Textile Foam Dyeing and Finishing. *Adv. Mater. Res.* **2011**, *332–334*, 1515–1519. [CrossRef]
8. Schelero, N.; von Klitzing, R. Ion specific effects in foam films. *Curr. Opin. Colloid Interface Sci.* **2015**, *20*, 124–129. [CrossRef]
9. Zhang, L.; Tian, L.; Du, H.; Rouzière, S.; Wang, N.; Salonen, A. Foams Stabilized by Surfactant Precipitates: Criteria for Ultrastability. *Langmuir* **2017**, *33*, 7305–7311. [CrossRef] [PubMed]
10. Zhang, L.; Wang, H.; Zheng, B.; Du, H.; Salonen, A. Surfactant Crystals as Stimulable Foam Stabilizers: Tuning Stability with Counterions. *J. Surfactants Deterg.* **2019**, *22*, 1237–1245. [CrossRef]
11. Binks, B.P.; Shi, H. Aqueous Foams in the Presence of Surfactant Crystals. *Langmuir* **2020**, *36*, 991–1002. [CrossRef] [PubMed]
12. Jiang, N.; Yu, X.; Sheng, Y.; Zong, R.; Li, C.; Lu, S. Role of salts in performance of foam stabilized with sodium dodecyl sulfate. *Chem. Eng. Sci.* **2020**, *216*, 115474. [CrossRef]
13. Chen, Y.; Ma, P.; Hu, K.; Cao, Y.; Chai, W. Insights into Flotation Separation of Dolomite from Magnesite with SDS Collector: Experiments and DFT Calculation. *Asia-Pac. J. Chem. Eng.* **2025**, *20*, e70028. [CrossRef]
14. Derjaguin, B.; Landau, L. The theory of stability of highly charged lyophobic sols and coalescence of highly charged particles in electrolyte solutions. *Acta Physicochim. URSS* **1941**, *14*, 58.
15. Verwey, E.J.W.; Overbeek, J.T.G. *Theory of the Stability of Lyophobic Colloids*; Elsevier: Amsterdam, The Netherlands, 1948; p. 218.
16. Verwey, E.J.W.; Overbeek, J.T.G. Theory of the stability of lyophobic colloids. *J. Colloid Sci.* **1955**, *10*, 224–225. [CrossRef]
17. Hofmeister, F. About regularities in the protein precipitating effects of salts and the relation of these effects with the physiological behaviour of salts. *Arch. Fuer Exp. Pathol. Und Pharmakol.* **1887**, *XXIV*, 247–260.
18. Hofmeister, F. About the water withdrawing effect of the salts. *Arch. Fuer Exp. Pathol. Pharmakol.* **1888**, *XXV*, 1–30.
19. Hofmeister, F. To the theory of the effect of the salts (First message). *Arch. Exp. Pathol. Pharmakol.* **1888**, *25*, 1–30.
20. Hofmeister, F. To the theory of the effect of the salts (Second message). *Arch. Exp. Pathol. Pharmakol.* **1888**, *24*, 247–260.
21. Collins, K.D. Charge density-dependent strength of hydration and biological structure. *Biophys. J.* **1997**, *72*, 65–76. [CrossRef] [PubMed]
22. Collins, K.D.; Neilson, G.W.; Enderby, J.E. Ions in water: Characterizing the forces that control chemical processes and biological structure. *Biophys. Chem.* **2007**, *128*, 95–104. [CrossRef] [PubMed]
23. Collins, K.D.; Washabaugh, M.W. The Hofmeister Effect and the Behavior of Water at Interfaces. *Q. Rev. Biophys.* **1985**, *18*, 323–422. [CrossRef] [PubMed]
24. Pitzer, K.S. Thermodynamics of electrolytes. I. Theoretical basis and general equations. *J. Phys. Chem.* **1973**, *77*, 268–277. [CrossRef]
25. Pitzer, K.S. *Activity Coefficients in Electrolyte Solutions*, 2nd ed.; CRC Press: Boca Raton, FL, USA, 1991.
26. Pitzer, K.S.; Mayorga, G. Thermodynamics of electrolytes. II. Activity and osmotic coefficients for strong electrolytes with one or both ions univalent. *J. Phys. Chem.* **1973**, *77*, 2300–2308. [CrossRef]
27. Pitzer, K.S.; Mayorga, G. Thermodynamics of electrolytes. III. Activity and osmotic coefficients for 2-2 electrolytes. *J. Solut. Chem.* **1974**, *3*, 539–546. [CrossRef]
28. Marcus, Y. Effect of Ions on the Structure of Water: Structure Making and Breaking. *Chem. Rev.* **2009**, *109*, 1346–1370. [CrossRef] [PubMed]
29. Marcus, Y. Specific ion effects on the surface tension and surface potential of aqueous electrolytes. *Curr. Opin. Colloid Interface Sci.* **2016**, *23*, 94–99. [CrossRef]
30. Marcus, Y. Prediction of salting-out and salting-in constants. *J. Mol. Liq.* **2013**, *177*, 7–10. [CrossRef]
31. Ni, N.; Yalkowsky, S.H. Prediction of Setschenow constants. *Int. J. Pharm.* **2003**, *254*, 167–172. [CrossRef] [PubMed]
32. Hummer, G.; Garde, S.; García, A.E.; Paulaitis, M.E.; Pratt, L.R. Hydrophobic Effects on a Molecular Scale. *J. Phys. Chem. B* **1998**, *102*, 10469–10482. [CrossRef]
33. Pandey, S.; Bagwe, R.P.; Shah, D.O. Effect of counterions on surface and foaming properties of dodecyl sulfate. *J. Colloid Interface Sci.* **2003**, *267*, 160–166. [CrossRef] [PubMed]
34. Marcus, Y. Ionic radii in aqueous solutions. *Chem. Rev.* **1988**, *88*, 1475–1498. [CrossRef]
35. Guven, O.; Batjargal, K.; Ozdemir, O.; Karakashev, S.I.; Grozev, N.A.; Boylu, F.; Çelik, M.S. Experimental Procedure for the Determination of the Critical Coalescence Concentration (CCC) of Simple Frothers. *Minerals* **2020**, *10*, 617. [CrossRef]
36. Çavdar, Y.E.; Karakashev, S.I.; Donchev, S.; Yotova, I.; Ozdemir, O. Ion-specific effects on the bubble coalescence in aqueous medium. *Physicochem. Probl. Miner. Process.* **2025**, *61*, 204586. [CrossRef]
37. Raykundaliya, N.; Parsana, V.M.; Grozev, N.A.; Mircheva, K.; Donchev, S.; Christov, C.; Karakashev, S.I.; Ivanova-Stancheva, D.; Yotova, I. Physicochemical vs. Chemical Pathways of Foam Inhibition: The Role of Cohesive Pressure and Specific Ion-Pairing. *Surfaces* **2026**, *9*, 36. [CrossRef]
38. Dack, M.R.J. The importance of solvent internal pressure and cohesion to solution phenomena. *Chem. Soc. Rev.* **1975**, *4*, 211–229. [CrossRef]
39. Long, F.A.; McDevit, W.F. Activity coefficients of nonelectrolyte solutes in aqueous salt solutions. *Chem. Rev.* **1952**, *51*, 119–169. [CrossRef]

40. Masterton, W.L.; Lee, T.P. Salting coefficients from scaled particle theory. *J. Phys. Chem.* **1970**, *74*, 1776–1782. [CrossRef]
41. Tanford, C. *The Hydrophobic Effect: Formation of Micelles and Biological Membranes*; John Wiley & Sons: New York, NY, USA, 1980; p. 687.
42. Lunkenheimer, K.; Czichocki, G.; Hirte, R.; Barzyk, W. Novel Results on the Adsorption of Ionic Surfactants at the Air/Water Interface—Sodium-N-Alkyl Sulfates. *Coll. Surf. A* **1995**, *101*, 187–197. [CrossRef]
43. Karakashev, S.I. How to determine the adsorption energy of the surfactant's hydrophilic head? How to estimate easily the surface activity of every simple surfactant? *J. Colloid Interface Sci.* **2014**, *432*, 98–104. [CrossRef] [PubMed]
44. Ivanov, I.B.; Ananthapadmanabhan, K.P.; Lips, A. Adsorption and structure of the adsorbed layer of ionic surfactants. *Adv. Colloid Interface Sci.* **2006**, *123–126*, 189–212. [CrossRef] [PubMed]
45. Ivanov, I.B.; Marinova, K.G.; Danov, K.D.; Dimitrova, D.; Ananthapadmanabhan, K.P.; Lips, A. Role of the counterions on the adsorption of ionic surfactants. *Adv. Colloid Interface Sci.* **2007**, *134–135*, 105–124. [CrossRef] [PubMed]
46. Slavchov, R.I.; Karakashev, S.I.; Ivanov, I.B. Ionic Surfactants and Ion-Specific Effects: Adsorption, Micellization, Thin Liquid Films. In *Surfactant Science and Technology: Retrospects and Prospects*; Romsted, L.S., Ed.; Taylor & Francis Group: Oxfordshire, UK, 2014; p. 593.
47. Marcelja, S. Selective Coalescence of Bubbles in Simple Electrolytes. *J. Phys. Chem. B* **2006**, *110*, 13062–13067. [CrossRef] [PubMed]
48. Leontidis, E. Chaotropic salts interacting with soft matter: Beyond the lyotropic series. *Curr. Opin. Colloid Interface Sci.* **2016**, *23*, 100–109. [CrossRef]
49. Lucassen-Reynders, E.H. *Anionic Surfactants*; Marcel Dekker: New York, NY, USA, 1981.
50. Alty, T. The Origin of the Electrical Charge on Small Particles in Water. *Proc. R. Soc. London. Ser. A Contain. Pap. A Math. Phys. Character* **1926**, *112*, 235–251. [CrossRef]
51. Firouzi, M.; Howes, T.; Nguyen, A.V. A quantitative review of the transition salt concentration for inhibiting bubble coalescence. *Adv. Colloid Interface Sci.* **2015**, *222*, 305–318. [CrossRef] [PubMed]
52. Henry, C.L.; Dalton, C.N.; Scruton, L.; Craig, V.S.J. Ion-Specific Coalescence of Bubbles in Mixed Electrolyte Solutions. *J. Phys. Chem. C* **2007**, *111*, 1015–1023. [CrossRef]
53. Craig, V.S.J. Bubble coalescence and specific-ion effects. *Curr. Opin. Colloid Interface Sci.* **2004**, *9*, 178–184. [CrossRef]
54. Bikerman, J.J. The unit of foaminess. *Trans. Faraday Soc.* **1938**, *34*, 634–638. [CrossRef]